Received: 18 May 2024 | Revised: 11 October 2024 | Accepted: 12 October 2024

DOI: 10.1002/pamm.202400107

PAMM Proceedings in Applied Mathematics and Mechanics

RESEARCH ARTICLE

Shape design optimization of a flat endmill tool

Abraham Kalu-Uka[1] | **Kevin Moerman**[2] | **Peter Eberhard**[1]

[1]Institute of Engineering and Computational Mechanics, University of Stuttgart, Stuttgart, Germany

[2]Department of Mechanical Engineering, University of Galway, Galway, Ireland

Correspondence
Abraham Kalu-Uka, Institute of Engineering and Computational Mechanics, University of Stuttgart, Germany.
Email: abraham.kalu-uka@itm.uni-stuttgart.de

Funding information
University of Stuttgart, Institute of Engineering and Computational Mechanics

Abstract

Among the many possible metal-cutting processes, milling is regarded as one of the most widely applied processes to machine different engineering materials productively. During the milling process, there is relative motion between the endmill tool and the workpiece. Energy is required to drive the cutting force used by the tool in separating the chips from the workpiece. Several studies have focused on the effects of milling process parameters on the cutting force, for instance by varying the cutting parameters, machining properties and the extent of cooling/lubrication. Other studies have explored the influence of tool geometry and material properties on the cutting force. Results from these studies have brought about improvements in the design of milling machinery and tools. The current study presents a novel automated approach for tool geometry optimization which is fully coded in Matlab. An automated and parametrized endmill design procedure was created featuring input parameters such as rake angle, relief angle, clearance angle and helix angle, all of which have been shown, through numerous studies, to influence cutting forces. The parameters were here used to generate the shape profile for one cutting edge of a flat endmill. This cutting edge profile is next copied and rotated, as per the design's pitch angle, to form the complete set of cutting flutes for the flat endmill. Next, the surface defined by the completed profile is meshed using quadrilateral elements. The 3D endmill design is then formed by extruding, and twisting as per the helix angle, this quadrilateral mesh to form a solid hexahedral mesh. Finally, an automated iterative optimization process was defined, featuring the above parametrized design process coupled with Abaqus-based finite element simulation of the milling process. The expected result is that the proposed optimization procedure will be able to identify the endmill design parameters which minimize the cutting force. At the completion of the optimization, a minimized maximum resultant cutting force value is obtained from using the newly optimized endmill. The resultant cutting force was reduced by 17.6%. It is anticipated that the automated design, meshing and simulation-driven optimization approach is generalizable to other tool design variations.

KEYWORDS
end milling, finite element simulation, meshing, optimization, shape parameters, spline control points

1 | INTRODUCTION

Milling is regarded as one of the most applicable processes for effectively machining a wide range of engineering materials. During milling, a workpiece is fed against a rotating tool with two or more cutting edges [1]. The process of physically separating a solid object into two or more parts is based on plastic deformation and the occurrence of fracture. This is why machining is considered to be the intentional fracturing of the removed layer [2]. The physical separation (in the form of chips) is the major difference between machining and other metal working processes [3]. The mechanisms through which milling is carried out, is outlined in the following procedures:

1. The material removal occurs on the circumference of the milling cutter with one or multiple cutting edges, which move perpendicular to the axis of the workpiece.
2. The machining starts as soon as the milling cutters enter the workpiece, and the multiple cutting edges of the milling cutter penetrate the workpiece and shave off the chips.
3. The chips are formed due to shear deformation, as the material is pushed off from the workpiece into tiny clumps which combine to a greater or lesser extent.

Chip removal during machining is a technique that has been used for many years but because of the varied set of factors (cutting conditions, tool, materials, etc.) which are involved, carrying out optimization on machining is still rarely applied. As a result, much research work needs to still be done in this area. Such a research study is important especially when the machined material, Titanium alloy (Ti6Al4V), has wide applications in aeronautic industries and is difficult-to-cut [4, 5]. It is also important to point out that conventional research of optimal milling process condition for this alloy has been done by trial and error most of the time and has often been found to be difficult and time consuming [6].

The tool used for milling is called an endmill or a cutter. It has sharp cutting edges that slice through a workpiece in a rotating motion along the milling cutting path. According to ref. [7], important shape elements of an endmill include the rake angle, relief angle and clearance angle. These interrelated elements along with the helix angle are the major geometric shape determinants of machinability. From recent milling process review studies [1], it can be understood that although tool geometry, as a factor in machining, has been the focus of a considerable number of research studies, yet it pales in comparison with the numerous number of studies that have dealt with machining characteristics like cutting speed, cutting depth, feed rate, lubrication and so forth. There are even fewer research studies on the optimization of milling processes with tool geometry parameters as optimization variables in spite of the effects on milling characteristics they have been found to have. For instance, the helix angle smoothens and extends the duration and geometric length of contact between a cutting edge and workpiece. Increasing both the helix angle and number of teeth reduces the stress on the tool [8]. The rake angle affects how sharp the cutting edge is and how easy it is to cut through the workpiece. It has an inverse connection with machining characteristics such as cutting forces or temperature. As the rake angle increases, the magnitude of cutting forces and temperature decreases [9]. The relief angle determines how much friction occurs between the cutting edge and workpiece while the clearance angle also acts like the relief angle but defines friction between the flank face of the cutting edge and the workpiece. When all these effects are summed together, they demonstrate how much critical influence an endmill's shape geometrical parameters have on the milling process.

Many experimental studies on the effects of tool shape geometric parameters have been undertaken. They are usually based on arbitrary variations of some parameter(s) and for the purpose of finding out their effects on milling. Despite the benefits that come with this study approach, it is expensive and time-consuming to analyse the different experimental-based studies in the milling process on complex machine parts [10] in this manner. More than 3 decades ago, research studies focused on 2D Finite Element Method (FEM) simulations of orthogonal cutting and later used 3D FEM models representative of oblique cutting to model various machining operations [1]. The application of FEM in recent years has helped to decrease the costs associated with milling and has provided accurate predictions of a variety of milling properties like stresses, strains, cutting forces, temperature and so forth, some of which (e.g., stress) are very difficult to obtain by experiments. A finite element modelling is a research methodology whereby the mechanics of metal cutting and prediction of various machining characteristics are carried out without regard to experiments. Nowadays, this study method has been deemed the best and most suitable with regards to computational time and robust calculations based algorithms [1]. In addition, studies have shown that the finite element approach is also able to predict the different machining characteristics, microstructure, effect of lubricants/coolants, tool wear and so forth. [1]

Various finite element-related studies have considered the different effects of the milling characteristics in milling Ti6Al4V on milling properties. Some of them investigated the effects of milling process parameters and include studies on effects of cutting parameters, machining properties, lubrication, varied tool shape parameters. These studies were carried out to predict properties that are associated with machining like cutting force, cutting temperature, surface roughness, tool wear, chip morphology, stresses, cutting energy/power, circularity (turn-milling), material removal rate, contact pressure, microstructure and vibration chatter [8, 11, 12]. Most of them were interested in the effects of the machining characteristics on cutting forces and or cutting temperature while a few others considered the effects of variations in the geometric shape parameters of a milling tool. A summary of some of these studies are hereby outlined.

The results obtained from the investigations carried out by Sima [13] on serrated chip formation during Ti6Al4V milling showed, that while the increase in spindle speed brings about an increase in the cutting force, decrease in rake angle decreases the thrust forces. Zhang et al.[2] examined the development of shear stress at the secondary deformation zone during the machining of Ti6Al4V alloy. It was found that an increase in the coefficient of friction decreases the cutting forces. Fu et al.[14] investigated FEM for cutting forces and examined the model for the end milling process. It was determined that in order to predict the milling forces, the milling type, the properties of workpiece material and the cutting tool geometry should serve as possible input data for the model. The Advant Edge FEM analysis tool was used for this oblique cutting milling process. A 3D model was created in Ducobu et al. [15] for orthogonal cutting using the coupled Eulerian–Lagrangian mesh formulation, and it was found that their increasing the width of the workpiece would lead to the meeting of the reference experimental values for cutting forces. The cutting tool geometries such as cutting edge, rake angle, circle segment radius, helix angle, number of teeth and tool orientation angle have a major influence on cutting forces according to Chauhan et al.[1]. A finite element analysis on the effects of variations in the helix profiles of an endmill was shown in Kalu-Uka et al. [16]. The result was a decrease in both stresses and cutting forces for the tool with helix profile variations compared with a regular endmill with constant helix angle. An investigation on the effect of minimum uncut chip thickness as a result of round edge cutting tool in the milling process has been done in Malekian et al. [17]. There were reported variations of cutting forces because of the piled up chip material in front of the cutting tool edge. In addition, at an excessive depth of cut, the ratio between the cutting force and thrust force was slightly decreased, which brought about a minimum uncut chip thickness relative to the cutting edge radius. In Hall et al. [9], numerical and experimental studies on the effect of the rake angle of a cutting tool during the milling of Ti6Al4V alloy were described. The study revealed that increase in rake angle leads to a decrease in the cutting forces and the minimum cutting force corresponded to a 14° rake angle. The model predicted the chip morphology behaviour to a limited extent as a result of varying the rake angle, which leads to increased chip thickness, decreased peak-to-valley ratio and mean pitch. An examination of the effect of cutting tool geometries on hard milling operations was carried and it was discovered that with increase in the depth of cut, the thermo-mechanical load increases [18]. The thermal and mechanical load can be decreased, by decreasing the maximum chip thickness and increasing the rotation angle. Pelayo [8] designed the time domain model that analyses the static and dynamic behaviour of a cutting tool. Increasing the helix angle reduces the cutting forces and then increasing the depth of cut and feed rate, brings about an increase in the cutting forces. The finite element analysis of micro-endmilling of Ti6Al4V was studied in Thepsonthi [19] and showed that the results from 2D and 3D simulations were the same. A relationship between negative rake with shear angle, shear zone and cutting forces was established. Negative rake angles increase the shear angle and magnify the shear zone thus leading to increased resistance to plastic deformation and then increased cutting forces.

Some other studies considered the effect of material deformation constitutive parameters, fracture and lubrication on cutting forces. Research works like [4, 10, 20] studied the effects of various deformation behaviour of Ti6Al4V alloy with respect to their material constitutive deformation properties, on stresses and cutting forces. Rech et al. [21] investigated the effects of friction and heat partition at the work and tool interface during milling process and stated that the friction models were reliant on cutting speed and thus affect cutting forces. Wu et al. [22] found out that the cutting force coefficient increases with the radial depth of cut from their developed FEM for cutting force prediction in an end milling process. Puls et al. [23] carried out experiments which varied metal conditions and studied their effects on friction and cutting forces. They presented that the cutting process passed through three stages. In the first stage, the cutting forces increase consistently until the cutter gets to the 8-mm mark from where the second stage begins. In this stage, the forces are constant. In the third stage, the forces decrease continually as a result of the disengagement of the cutter from the

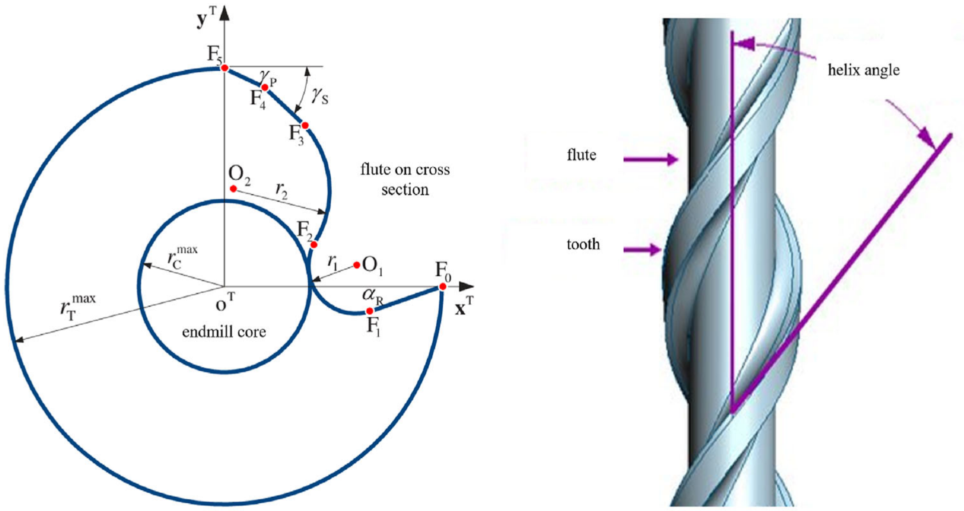

(A) endmill cross section geometry, [27] (B) endmill longitudinal view showing helix angle, [28]

FIGURE 1 A typical endmill tool geometry.

workpiece. Melkote et al. [24] reviewed the various advances in constitutive and friction models for simulating metal machining. They asserted that the friction model is developed by cutting forces which were affected by the work material and its microstructure, cutting speed, cutting fluid and tool cuttings.

Lubrication can strongly affect cutting forces because lubricants generally decrease cutting friction while extending the tool life [1]. A finite element model was used in Davoudinejad et al. [25] to compare the dry and cryogenic cooling for Ti6Al4V alloy machining. It was observed that the high cooling effect of the cryogenic coolant causes hardening on the workpiece thereby increasing the force required to cut through it. He et al. [26] also compared the cryogenic and dry machining of Inconel 718, and found that there was relatively no change in the cutting forces in both cases.

In spite of all the studies already discussed, there is still a knowledge gap that needs to be filled in executing a systematic optimization study that integrates the finite element method with the coupling of an optimization solver. Efforts to fill this gap would involve carrying out a cutting force optimization study together with FEM simulations using Abaqus, on the shape profile parameters of a flat end mill. Shape parameters which are studied include the rake angle, rake face, clearance angle, clearance side, relief angle, relief side, helix angle as well as the control points that run through the free curve connecting the end of the rake side to the beginning of the clearance side. In the present study, the geometric shape parameters would be used in designing an endmill tool model. Through a defined automated iterative optimization process, featuring the parametrized design process coupled with Abaqus-based finite element simulation of the milling process, the endmill design parameters which minimize the cutting force will be identified.

2 | METHODOLOGY

2.1 | Endmill geometry

In Figure 1a, the axial cross section of an endmill is shown, with the points F_0, F_1, F_2, F_3, F_4 and F_5 been used in tracing a typical endmill profile. They correspond to the red points seen on Figure 2b. The endmill's relief, clearance and rake angles are represented by γ_p, γ_s and α_R while r_c and r_c are the inner and outer radii of a typical endmill. Other important shape parameters like the flute, tooth and helix angle are shown in Figure 1b. For creating an endmill cutting profile, the following procedures can be followed:

1. Using analytical equations and established constraints for a curved section of the endmill profile, a set of points which defines the profile is generated, see Figure 2a.
2. A cubic interpolating spline is applied to connect the curved part of the profile (from the end of the non arrow tipped side of the rake face F_1, through the central point F_2 that determines the helical groove, to the beginning of the clearance face at F_3. The curve region marked with the blue line is the part of the curve created with the spline. Along this blue

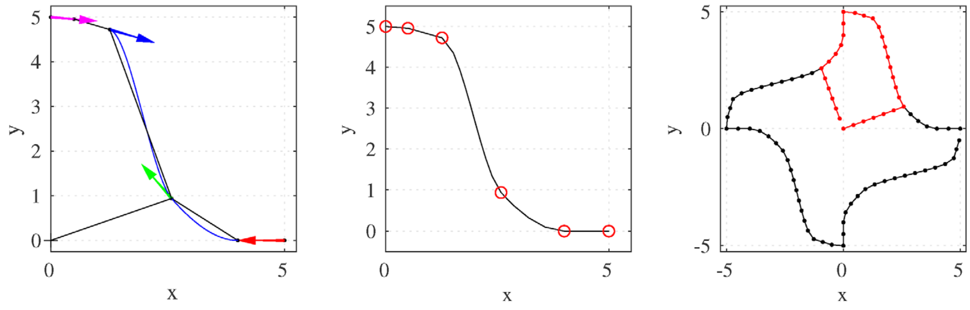

(A) Endmill curve profile segment (B) Curve profile segment with parametric points (C) Endmill curve profile cross-section

FIGURE 2 Step-by-step development of an endmill's closed curve profile generation.

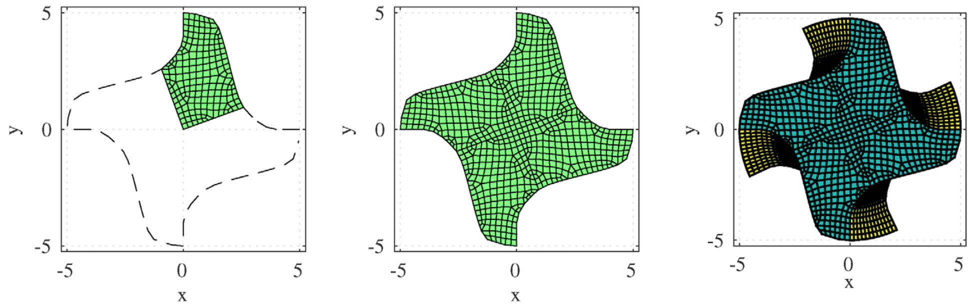

(A) Systematic segment meshing (B) Mesh for endmill curve profile cross-section (C) Solid extruded mesh

FIGURE 3 Step-by-step development of an endmill's full curve mesh generation.

line, constraints like monotonicity and smoothness are imposed on absolute valued control points. The lines of the left facing red arrow, the right facing pink arrow and the right facing green arrow, represent the rake face, relief side and clearance side of the endmill respectively. The dimensions of these lines, their corresponding angles and the control points along the blue curve region, serve as variables for an optimization process.

3. Dimensional vectors are introduced along the rake face, relief and clearance sides, see Figure 2a. This is to ensure that there is c continuity at the start and end points of the curves meeting at these points.
4. With the curve profile now determined, see Figure 2b, multiple curve profile points are generated which form the vertices to be used for developing the mesh.
5. The single cutting edge profile is copied and rotated, as per the design's pitch angle, to form a closed curve. This copying depends on the number, n of cutting flutes (edges) the flat endmill is expected to have, see Figure 2c. This is determined using the pitch angle, θ and is expressed as $n = 360/\theta$.

2.2 | Endmill meshing

The area under the closed curve, Figure 2c is meshed with the application of the Gibbon code [29]; a robust meshing tool. It is an open-source Matlab toolbox that is interfaced with a free open-source software used in robust geometry meshing for finite element analysis. Because the meshing, nodes or elements affect the computational time, machining characteristics, accuracy and the simulation results of FEM, it is important to have a mesh generator that can be flexibly adapted to generate a good mesh during each optimization step. Gibbon code has the capability to do this and is also equipped with the language program code structure for preparing and writing the Abaqus input files for different engineering processes. It is also coupled with the Febio application, a finite element analysis tool used in biomedical engineering simulations. Thus, in applying this code to the segmented area bounded by red points in Figure 2c; the surface defined by the completed profile is first meshed using quadrilateral elements, see Figure 3a. This style of meshing starts from the centre point of the geometry and it has an important advantage. It is easy to pick out the reference point node that would be used for the

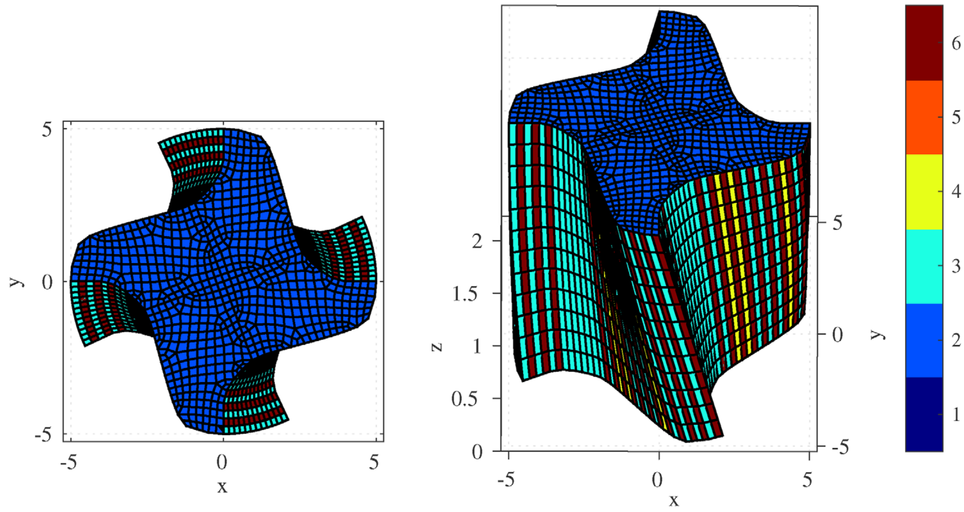

(A) view from the top surface

(B) side view showing the different sides-surfaces

FIGURE 4 Abaqus contact surfaces' definition.

angular velocity boundary condition which is responsible for the rotatory movement of the endmill too. This also makes it possible to carry out a milling optimization process in which the mesh of the tool changes with each optimization step, but still the reference point node location remains the same. Next, this segment is mesh-multiplied over the number of cutting flutes until the whole cross section is meshed, Figure 3b. The 3D endmill design is then formed by extruding, and twisting as per the helix angle, to form a solid hexahedral meshed endmill. The cubic workpiece geometry is created and also meshed with hexahedral elements, see Figure 3c. Both endmill tool and workpiece are then assembled to set them up in a milling position.

Abaqus has a specific way of defining mesh surfaces that should be followed when the input files have to be coded in an environment that is outside Abaqus. This is important to ensure that contact definitions between tool and workpiece are accurately executed, see Figure 4a and b. The legend shows the surfaces of the mesh that must be defined. 1 and 2 stand for the top and bottom surfaces while 3, 4 and 6 are for the side-surfaces. It can be observed that there is no side-surface 5 because its orange colour is not represented on the endmill's sides surfaces. It is to be pointed out that all the entries in the legend are not always represented. However, with more complex shapes, side-surface 5 becomes visible for example, when the cutting edges are increased to five flutes. (N

A thermo-mechanical finite element model is developed using the commercial software Abaqus/Explicit 2020. It consists of a three-dimensional oblique cutting model in plane strain condition. The machined workpiece material is Ti6Al4V, a titanium alloy and the tool material is P20 Mold steel. P20 was chosen because of its ability to transfer heat away from the chip tool contact as a result of having a good thermal conductivity [30]. This choice is important as it ensures that the tool is thermally stable and would not break down at elevated temperatures. Gibbon code is used again to write the Abaqus input file within the Matlab programming environment. This input file contains information about the nodes, elements, contact, boundary conditions and so forth (which are required for a milling simulation process) into an Abaqus input file. The completed input file can now be fed to an Abaqus finite element processor to carry out a milling process simulation

Other important information about the geometry and mesh are also provided. The dimensions of the workpiece are 6 mm × 2 mm × 0.5 mm. The numerical model for the workpiece is made up of 19 040 hexahedral elements, and the element type is C3D8RT. The endmill is made up of 4 flutes (for a pitch angle of 90°). Four (4) flutes were chosen based on the results from Denkena et al. [31] where it was stated that cutting forces were maximum in single tooth cutters and minimum with four tooth cutters. The endmill has inner and outer (main) diameters of 10 and 5.50 mm. The height of the tool is 2 mm. For the shape parameters of the initial design, the helix angle is 25°, the rake angle is 0°, the relief angle is 5° and the clearance angle is 17°. The model of the tool is set to rigid and the tool has 8352 hexahedral elements of element type C3D8RT (8-node thermally coupled brick, trilinear displacement and temperature, reduced integration, hourglass control). The axial depth of cut is 0.5 mm while the radial depth of cut is set to 0.1 mm. The time integration method used is dynamic temperature displacement explicit that could determine the stress distribution, reaction cutting forces and milling temperature. In the tool-workpiece assembly, the bottom and adjacent ends are firmly fixed in position using

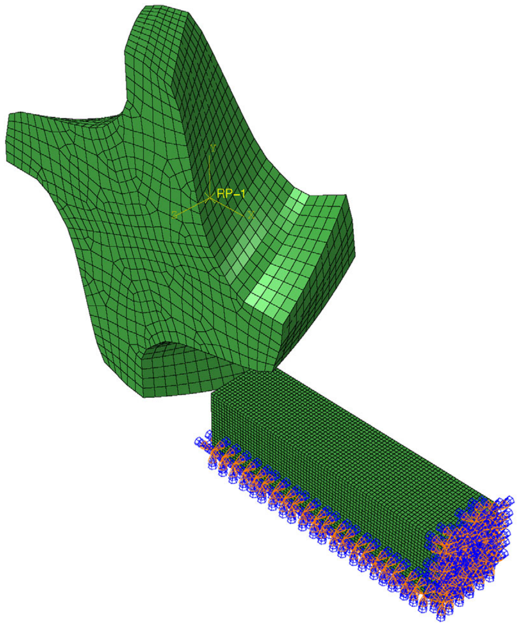

FIGURE 5 Tool and workpiece assembly.

TABLE 1 Physical properties of Ti6Al4V alloy workpiece [2].

Density (kg/m^3)	Youngs modulus (GPA)	Poisson ratio	Thermal conductivity (W/mK)	Linear expansivity ($10^-6/^0C$)	Specific heat capacity (kJ/kg)
4430	110	0.33	6.6	9	670

TABLE 2 Physical properties of P20 steel endmill [30].

Density (kg/m^3)	Youngs modulus (GPA)	Poisson ratio	Thermal conductivity (W/mK)	Linear expansivity ($10^-6/^0C$)	Specific heat capacity (kJ/kg)
15700	705	0.23	24	5	178

the Encastre boundary condition while the tool rotates and moves against the workpiece with a given spindle and feed speeds, see Figure 5. The spindle speed is 109 rad/s while the effective feed rate is 90 mm/s. See Tables 1 and 2 for the thermo-mechanical properties of the workpiece and endmill materials respectively.

2.3 | Results processing

After a simulation run is completed, it is necessary to have an automatic process where the results from Abaqus simulation are collected without having to manually open the Abaqus' output database (ODB) file using the Graphic User Interface (GUI) to view and obtain the results as is normally done. This is impracticable for an optimization process which requires multiple runs and requires a Matlab system that automatically returns values of the the criterion value. Thus to ensure that there is no interruption that requires manual intervention and to allow the optimization to run seamlessly until completion, the Abaqus2Matlab function is coupled to the optimization processso as to process the results from the output file created after every simulation. The required milling property results, for example: cutting forces, cutting temperature (possible criterion values) etc. can be extracted at specific nodes using this function. Abaqus2Matlab [32] is an open-source Matlab toolbox that establishes an interface connection between Abaqus and Matlab. For carrying out contact simulations, Abaqus2Matlab largely encourages structural integrity assessment by taking advantage of advanced damage models found in Abaqus and modern optimization abilities of Matlab. Furthermore, its application can be easily widened to a vast range of non linear problems, in which inverse analysis is an invaluable tool. The ability of Abaqus2Matlab to do all these, gives rise to new possibilities in results post-processing, statistical analysis and mathematical optimization. Results processing can be done by using the function to first process initial Abaqus results file (.fil) into either a binary or American Standard Code for Information Interchange, (ASCII), format file, depending on the format the file results are required to be in while moving the results between different operating systems. For this study, the more convenient ASCII format is chosen due to its versatility and readability. To ensure that the results can be successfully collected using Abaqus2Matlab, specific options in the input (.inp) file that carry out the required commands are included when writing the file. The results file generation procedure is different for operations involving Abaqus/Standard or Abaqus/Explicit, respectively. In the former, *FILE FORMAT, ASCII must be specified in the former and *FILE OUTPUT in the latter. File output types included element, nodal, energy, modal, contact surface, element matrix, and so forth can be written to the results file.

2.4 | Optimization model

Typically, structural optimization falls into three categories: sizing, shape and topology optimization. Sizing optimization is aimed at determining the optimum thickness or cross-sectional area of a structural member for the sake of minimizing cost or maximizing design of performance. In shape optimization, there is the intention to bring about smooth modifications of domain boundaries to find out optimum geometric profile when design topology remains fixed. Topology optimization operates with maximizing design flexibility and determination of the optimal material. distribution through creating and merging holes in the structure [33, 34]. When compared, shape optimization is taken to be more significant with respect to sizing optimization because it brings about better structural properties like stress distribution and structural weight. During a shape optimization process, the design domain keeps on changing through design variable updates and subsequent internal and or external boundary variations [34]. Shape optimization can be defined as an iterative process of determining optimum geometric configuration by integrating design, analysis and optimization activities under prescribed design constraints [6].

Shape optimization procedures can be grouped into parametric or non-parametric approaches. The parametric approach can be linked to Computate Aided Design (CAD) geometry in which a set of geometric parameters like angles, distances, radii and so on are used to define the shape. The parametric method looks for the space covered by the constrained design variables in order to minimize or maximize the externally defined objective function. On the other hand, the non-parametric approach represents the geometry by the nodal positions of surface nodes in an FE model. Throughout the optimization process, the nodal positions are updated by displacing the nodes along the direction of predetermined displacement vectors. This method makes it possible to modify every node of a set of design nodes during optimization. It is parameter free. However, it has several significant disadvantages. There is the problem of increased number of design variables which leads to increased computational time and the possibility of getting unrealistic and jagged geometric shapes which are meaningless. This arises because of the non-smooth nature of shape derivatives.

To optimize engineering systems/structures, contemporary numerical techniques like FEM, Boundary Element Method (BEM), Computational Fluid Dynamics (CFD) and newer techniques like meshless methods (MM) and Iso-Geometric Analysis (IGA) are coupled with deterministic and stochastic optimization algorithms [6]. Particle Swarm Optimization (PSO) from [35] is employed in this study for running the optimization process. The PSO is a stochastic optimization method based on the simulation of the social behaviour of bird flocks or fish schools. It is similar to evolutionary algorithms as it is a population-based algorithm. Its algorithm makes use of swarm intelligence to find the best place in the search space. Using a particular design vector $\boldsymbol{x}$ that describes the real position of a particle in the design search space, the trajectory of the i-th particle at iteration k can be described with the position update equation

$$\boldsymbol{x}_i{}^{k+1} = \boldsymbol{x}_i{}^{k} + \Delta\boldsymbol{x}_i{}^{k+1} \tag{1}$$

and the so-called velocity update equation is

$$\Delta\boldsymbol{x}_i{}^{k+1} = w\Delta\boldsymbol{x}_i{}^{k} + c_1 r_{1,i}^{k}\left(\boldsymbol{x}_i^{best,k} - \boldsymbol{x}_i{}^{k}\right) + c_2 r_{2,i}^{k}\left(\boldsymbol{x}_{swarm}^{best,k} - \boldsymbol{x}_i{}^{k}\right) \tag{2}$$

where the position change $\Delta\boldsymbol{x}_i{}^{k+1}$ is usually referred to as ”velocity”. Though this is physically incorrect, it is the traditional terminology used in literature. Mathematically, the unit used for position change (displacement) is not the same as the unit for velocity. However, ”velocity” is used here as a metaphor to describe the rate and direction of a particle's change in position within a search space. w stands for the inertia factor. $\boldsymbol{x}_i{}^{best,k}$ is the best previously determined position of

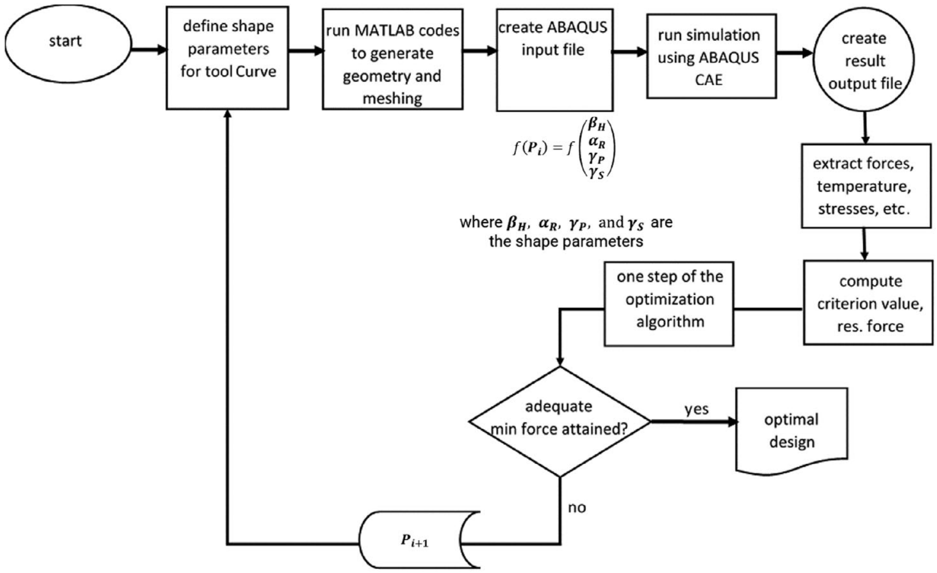

FIGURE 6 Flow chart that summarizes the optimization process.

the particle i and $\boldsymbol{x}_{swarm}^{best,k}$ is the best position in the entire swarm at the current iteration k. $r_{1,i}^k$ and $r_{2,i}^k$ are uniformly distributed random numbers in [0,1] and stand for the stochastic behaviour of the algorithm. The choice of the control parameters c_1 and c_2 are made to attain convergence. The term $c_1 r_{1,i}^k \left(\boldsymbol{x}_i^{best,k} - \boldsymbol{x}_i{}^k\right)$ is associated with cognition, because it considers only the best position of the particle's own experience. The social interaction of the particles is represented by $c_2 r_{2,i}^k \left(\boldsymbol{x}_{swarm}^{best,k} - \boldsymbol{x}_i{}^k\right)$. c_1 and c_2 are called the cognitive scaling factor and social scaling factor respectively. Along with the inertia factor w, they influence the particle trajectories and thus the behaviour of all the swarm. They can be used to control the behaviour of the swarm, particularly with respect to the convergence and search diversity properties of the algorithm. Applying Equations (1) and (2) iteratively to a set of n_p particles (swarm), the basic PSO algorithm comprises the following steps:

1. Initialize n_p particles with predefined or randomly chosen positions and determine corresponding objective function values at each position. Set $k = 0$. Determine $\boldsymbol{x}_i{}^{best,0}$ and $\boldsymbol{x}_{swarm}^{best,0}$.
2. Check termination criteria. If it is satisfied, the algorithm comes to an end with the solution $\boldsymbol{x}^* = \boldsymbol{x}_{swarm}^{best,k}$.
3. Apply update Equations (1) and (2) to all particles and evaluate corresponding objective function values at each position. Set $k = k + 1$. Determine $\boldsymbol{x}_i{}^{best,k}$ and $\boldsymbol{x}_{swarm}^{best,k}$.
4. Go on to step 2.

The summary of all the steps involved in the optimization of the maximum resultant cutting force for an endmilling process is given in Figure 6.

For the optimization study, the maximum resultant cutting force is the criterion value. It is the highest value that is obtained from the resultant of the feed forces, axial forces and feed normal forces at each time step. It is adopted as a criterion value because it takes into consideration the contribution of all the forces in action during a milling process. Minimizing this value is thus the objective of the optimization process. The parameters to be optimized are: helix angle β_H, rake angle α_R, relief angle γ_P and clearance angle γ_S. The objective for the optimization process (with the boundary constraints) is

$$\begin{aligned} &\textbf{minimize} \quad \text{maximum resultant cutting force} \\ &\text{subject to: } 1.0^0 \leq \boldsymbol{\beta} \leq 55^0 \\ &-15^0 \leq \boldsymbol{\alpha} \leq 30^0 \\ &0.5^0 \leq \boldsymbol{\rho} \leq 30^0 \\ &0.5^0 \leq \boldsymbol{\gamma} \leq 40^0 \end{aligned} \tag{3}$$

TABLE 3 Parameters of Johnson–Cook constitutive equation for Ti6Al4V alloy [2].

A (MPa)	B (MPa)	C	n	m	$\hat{\epsilon_0}$
1098	1092	0.014	0.93	1.1	1

TABLE 4 Parameters of Johnson–Cook damage (fracture) for Ti6Al4V alloy [2].

D_1	D_2	D_3	D_4	D_5	$\hat{\epsilon_0}$
−0.09	0.25	−0.5	0.014	3.87	1

2.5 | Material constitutive equation, damage criterion and friction model

2.5.1 | Johnson–Cook material model

Modelling of the metal cutting processes in the absence of a proper material constitutive model that includes fracture induces unrealistic behaviour. To deal with this challenge, the information of the material constitutive behaviour under severe loading conditions is applied [11]. The Johnson-Cook (JC) material law, which is applicable to dynamic problems involving large deformations and high strain rate temperature effects, is used in this simulation to describe Ti6Al4V deformation process. This material law gives the expression for the flow stress that occurs during plastic deformation and has been widely applied in numerical studies for deformation processes [10]. It describes the stress–strain response along with the strain hardening effects, strain rate hardening and thermal softening. The flow stress is

$$\sigma = (A + B\epsilon^n)\left[1 + C\left(\ln\frac{\hat{\epsilon}}{\hat{\epsilon_0}}\right)\right]\left[1 - \left(\frac{T - T_0}{T_m - T_0}\right)^m\right] \quad , \tag{4}$$

where A, B, C, m, n represent the initial yield stress, hardening modulus, strain rate sensitivity coefficient, work hardening exponent and thermal softening coefficient, respectively. The equivalent stress is σ, ϵ is the equivalent plastic strain, $\hat{\epsilon}$ is the equivalent plastic strain rate, $\hat{\epsilon_0}$ is the reference plastic strain rate, T_0 is the reference temperature, T_m is the melting temperature and T is the temperature in the material cutting zone. See Table 3 for the values of the JC parameters for Ti6Al4V.

2.5.2 | Johnson–Cook damage evolution criterion

An appropriate modelling of work material for machining takes into consideration not only the determination of the material flow stress under similar conditions as those observed in machining but also under which conditions the fracture would occur and how to model it adequately [2]. To account for fracture or damage in the material, the JC damage evolution criterion is used. This criterion gives the expression for the equivalent plastic strain which describes the influence of strain, strain rate and temperature, in bringing about material fracture. When the equivalent plastic strain attains a certain criteria value required for material separation from the workpiece, damage initiation takes place, which leads to chip formation.The JC damage evolution criterion is

$$\epsilon_f = \left(D_1 + D_2 \exp\left(-D_3\frac{p}{q}\right)\right)\left[1 + D_4 \ln\frac{\hat{\epsilon}}{\hat{\epsilon_0}}\right]\left[1 + D_5\left(\frac{T - T_0}{T_m - T_0}\right)\right] \quad , \tag{5}$$

where D_1, D_2, D_3, D_4 and D_5 are initial failure strain, exponent factor, triaxiality factor, strain rate factor and temperature factor, respectively, and p is the hydrostatic pressure and q is the von Mises stress. Damage evolution is applied in Abaqus by inputing either equivalent plastic displacement or fracture energy dissipation [36]. See Table 4 for the damage values of Ti6Al4V.

2.5.3 | Coulomb's friction model

The Coulomb friction model is used to describe the contact interaction between the tool and developing chips. To apply this model, it is assumed that the frictional stress on the cutter is proportional to the normal stress with a constant friction coefficient. Two regions can be observed during contact: sliding and sticking, see [37]. The sliding region shows linear relation between frictional and normal stress, while in the sticking region, the shear stress is constant and equal to the critical stress.

1. for sticking,

$$\tau_f = k_c \quad \text{for} \quad \mu\sigma_n \geq k_c \tag{6}$$

2. for sliding,

$$\tau_f = \mu\sigma_n \quad \text{for} \quad \mu\sigma_n < k_c \tag{7}$$

where σ_n is the normal stress, τ_f is the frictional tangential stress, k_c is the shear flow stress of the material, and μ is the friction coefficient. For this study μ is 0.5 [37]. The value of the coefficient of friction is the most influencing factor during milling and presents some difficulties because it cannot be accurately measured [38]. Thus it should be chosen carefully.

2.5.4 | Lagrangian formulation and Abaqus analysis mode

To compute the mechanics behind the machining process, the applicable mesh formulations/models are Lagrangian, Eulerian and Arbitrary Lagrangian-Eulerian. Lagrangian-based models are very much used in machining operations simulation because of their ability to initially calculate chip morphology from the incipient stage to the steady state, where the chip shape forms as a result of cutting parameters, tool geometry, plastic deformation mechanism and tool-workpiece material characteristics. For the Eulerian-based models, the material flow is in a controlled volume together with the spatial fixed finite element mesh. When computation time needs to be minimized, the Eulerian-based model is recommended because it requires fewer mesh elements. In addition, the simulations for machining operations are set in order to get to steady-state conditions so there are no separation criteria in this model [1]. Other formulation variants exist that combine the advantages or characteristics of both already described formulations in different manners. This includes coupled Eulerian–Lagrangian (CEL) formulation and the Adaptive Lagrangian Eulerian (ALE) formulation. For oblique 3D cutting simulations, chips are expected to be produced. These chips are formed when there is separation between the elements of the meshed workpiece after deformation and fracture. The expectation of chips formation during milling simulation was the guiding factor in choosing Lagrangian formulation for this study.

During Abaqus analysis, two different modes can be applied: Abaqus/Standard or Abaqus/Explicit. Explicit is generally preferred during milling simulations because explicit analyses are sure to converge. The element deletion technique is used to allow element separation to take place during chip formation. Mass scaling, which is a numerical technique that permits the artificial acceleration of finite element calculations, was responsibly applied to balance accuracy of results with simulation time for each step of the optimization. For a total simulation time of 0.065 s, a discretization time step of 10^{-5} s is used.

3 | RESULTS AND DISCUSSION

The optimization process ended after 56 iterations and 586 function evaluations, see Figure 7. The minimized maximum resultant force was determined to be 97.28 N, a 17.6% decrease from the value obtained from the initial design; 118.12 N. This makes for a reduction of 20.84 N after optimization. With respect to the lower and upper boundary limits established for the optimization variables, see the bounds listing after Equation (3), the values; 5.5°, 27.5°, 24° and 1° were obtained for the helix, rake, relief and clearance angles after the optimization. These values are considerably different from the values

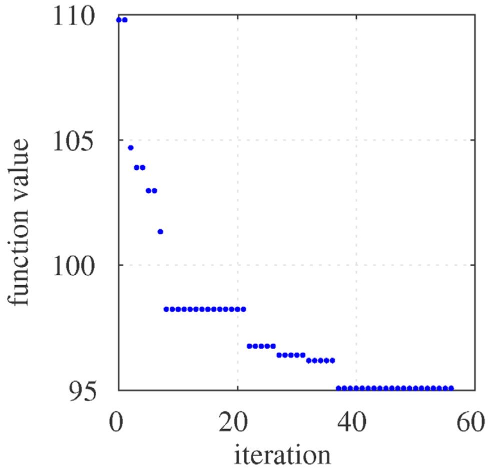

FIGURE 7 Optimization function plot with the best function value at 95.0747.

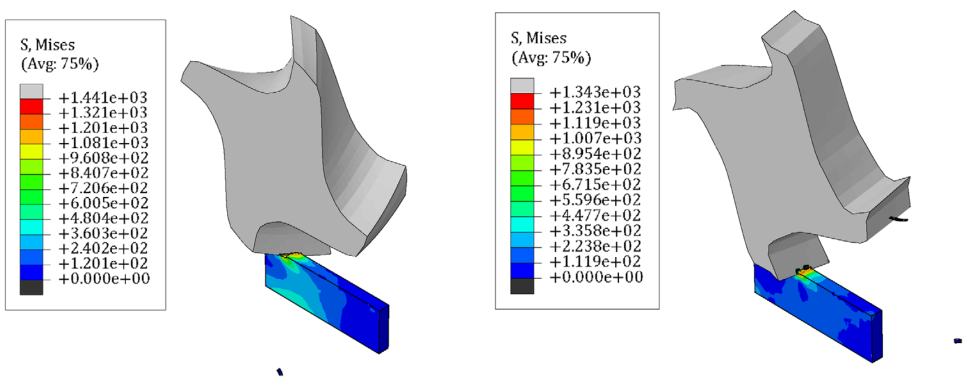

(A) milling with initial tool design

(B) milling with optimized tool design

FIGURE 8 Stress distribution of Ti6Al4V milling process for the initial and optimized cases during the 3rd cutting engagement through the workpiece.

used for the initial design: 25°, 0°, 5° and 17°. It is to be pointed out that none of these values lie on the lower or upper bounds that were set for the optimization process, thus providing some level of credibility to the optimization process. The obtained geometric shape parameters result in the design of an endmill that has sharp cutting edges, especially around the rake face and the relief side.

The simulation results in Figure 8 show the formation of chips with the conclusion of the second cutting engagement through the workpiece for both tools. The maximum von Mises stress values recorded throughout the simulations for the initial and optimal tool designs were 1.441 and 1.343kPa, respectively. This gives a reduction of 98kPa when milling with the optimal design. Milling with the initial design produced continuous chips which are not subject to breakage as seen in Figure 8a. The continuous chips which have been formed are unbroken and have the same width as the workpiece. In the optimal case in Figure 8b, the chips are seemingly broken up into smaller bits along the period of complete tool-workpiece engagement. Though continuous chip is often considered to be an ideal chip that generates relatively stable cutting forces, it is not acceptable for automated machining because they may disrupt the machining process. This might result in damage to the machined surface, cutting tool or machine tool [40]. To reduce these problems, segmented chips (some form of broken chips) are preferred [41].

The integral force is the value of the sum of all the forces recorded over the total simulation time. Even though the integral force value was not used as the optimization's criterion value, it is still an important factor to be used in comparing the performance of both the initial and the optimized tool designs. This is because of the possibility of having an occurrence where there could be a very high isolated peak maximum resultant force value during a particular cutting cycle whereas the other force peaks are much lower. Summing up all the force values over time thus gives a general overview of all the acting cutting forces during milling. The obtained value of the integral force for the initial tool design is 0.8314 Ns while

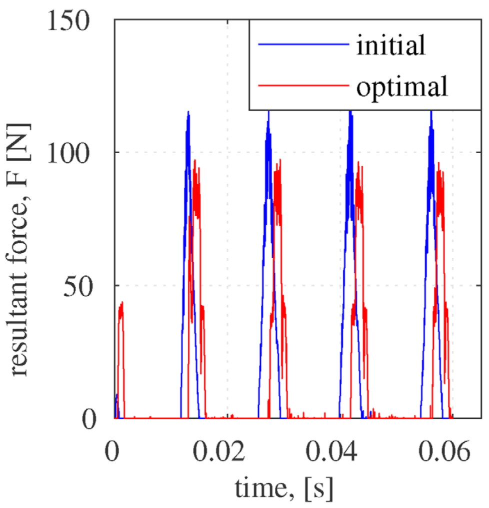

FIGURE 9 Maximum resultant cutting forces over time for initial and optimized cases.

that of the optimized tool is 0.7220 Ns. This represents a reduction of 13.15%. A possible explanation for this reduction can be found in the recurrent "thinning" of the optimized red curve profile between the regions where noise signals occur on the force-time plot of the milling process, just below the 50 N mark along the beginning and ending of each cut made by a cutting edge, see Figure 9. However, there is no thinning associated with the blue curve profile for the initial design. This thinning occurred in all the four cuts carried out by the respective 4 cutting edges of the optimized endmill and thus could be responsible for the reduction in the integral force value obtained for the optimized tool design.

It is to be pointed out that the profile of the optimal design in the resultant force against time plot in Figure 9, is not in the same phase with the initial design, but instead lags it. This situation persists in spite of setting the tool-workpiece assembly to have the same positioning, no matter what tool design (combination of optimization variables) is used during optimization. The reason for this lies with the shape of the optimal design. By virtue of its geometric parameters (angles) being markedly different from the initial design, the tool is automatically relatively positioned a bit closer to the workpiece. This new position causes a bigger first cut to be made on the workpiece (compared to the first cut from the initial design), before each of the other cutting edges of the endmill individually make their complete cutting engagements. Though, effort was made to add 0.25 mm tool-workpiece spacing to the original 0.1 mm setting, the lagging was still visible.

4 | CONCLUSION

An improved shape for a flat endmill tool has been put forward based on results from the particle swarm optimization process (maximum resultant cutting force was used as the criterion value) that was executed for this study. The optimal tool design demonstrated improvements in the milling process as evidenced in the reduced value of the maximum von Misses stress recorded for the optimal design. The resulting broken-up chips during milling with the optimal design, see Figure 8, are also preferable to the continuous segmented chips produced with the initial design. In addition, there was a 17.6% reduction in the maximum resultant cutting force for the optimal tool. It is anticipated that the automated design, meshing and simulation-driven optimization approach is generalizable to other tool design variations.

Further investigations can be carried out in the future by using the cutting temperature as the criterion value for another optimization process. It is also possible to undertake a multi-criterion optimization that combines the minimization of cutting force and cutting temperature at the same time. There is also the consideration of using the spline points of a cubic interpolating spline as the optimization variables instead of the geometric shape angles used in this study.

ACKNOWLEDGMENTS
The first author is thankful to and gratefully acknowledges the Deutscher Akademischer Austauschdienst (DAAD) for funding his research studies.

ORCID

Abraham Kalu-Uka https://orcid.org/0000-0002-4374-4961
Kevin Moerman https://orcid.org/0000-0003-3768-4269
Peter Eberhard https://orcid.org/0000-0003-1809-4407

REFERENCES

1. Chauhan, S., Trehan, R., & Singh, R. (2023). State of the art in finite element approaches for milling process: A review. *Advances in Manufacturing*, *11*, 708–751.
2. Zhang, Y., Outeiro, J., & Mabrouki, T. (2015). On the selection of Johnson-Cook constitutive model parameters for Ti6Al4V using three types of numerical models of orthogonal cutting. *Proceedings: 15th CIRP Conference on Modelling of Machining Operations*, Karlsruhe, Germany, CIRP 31 Elsevier, Karlsruhe, pp. 112–117.
3. Astakhov, V., & Shvets, S. (2004). The assessment of plastic deformation in metal cutting. *Journal of Material Processes and Technology*, *146*, 193–202.
4. Yaich, M., Ayed, Y., Bouaziz, Z., & Germain, G. (2017). Numerical analysis of constitutive coefficients effects on FE simulation of the 2D orthogonal cutting process: Application to the Ti6Al4V. *International Journal of Advanced Manufacturing Technology*, *93*, 283–303.
5. Ozel, T., & Sima, M. (2010). Finite element simulation of high speed machining Ti6Al4V alloy using modified material models. *Transactions of NAMRI/SME*, *38*, 49–56.
6. Ducobu, F., Riviere-Lorphevre, E., & Fillipi, E. (2015). On the introduction of adaptive mass scaling in a finite element model of Ti6Al4V orthogonal cutting. *Simulation Modelling Practice and Theory*, *53*, 1–14.
7. Kim, J., Park, J., & Ko, T. (2008). Endmill design and machining via cutting simulation. *Computer Aided Design*, *40*, 324–333.
8. Pelayo, G. (2019). Modelling of static and dynamic milling forces in inclined operations with circle-segment end mills. *Precision Engineering*, *56*, 123–135.
9. Hall, S., Loukaides, E., & Newman, S. (2020). Computational and experimental investigation of cutting tool geometry in machining titanium Ti-6Al4V. *Procedia CIRP*, *86*, 139–144.
10. Sekar, K. S., & Kumar, M. (2011). Finite element simulations of Ti6Al4V titanium alloy machining to assess material model parameters of the Johnson-Cook constitutive equation. *Journal of the Brazillian Society of Mechanical Sciences and Engineering*, *33*(2), 203–211.
11. Li, B., Zhang, S., & Zhang, J. (2019). Plastic deformation and grain refinement in surface layer induced by thermo-mechanical loads for hard milling process. *Proceedings of the Institute of Mechanical Engineering, Journal of Engineering Manufacture*, *233*(10), 2033–2046.
12. Tlhabadira, I., Daniyan, I., Masu, L., & Vanstaden, L. (2019). Process design and optimizaiton of surface roughness during M200 TS milling process using Taguchi method. *Procedia CIRP*, *84*, 868–873.
13. Sima, M. (2010). Modified material constitutive models for serrated chip formation simulations and experimental validation in machining of titanium alloy Ti6Al4V. *International Journal of Machining Tools and Manufacturing*, *50*, 943–960.
14. Fu, Z., Yang, W., & Wang, X. (2015). Analytical modelling of milling forces for helical end milling based on a predictive machining theory. *Procedia CIRP*, *31*(4), 258–263.
15. Ducobu, F., Riviere-Lorphevre, E., & Fillipi, E. (2017). Finite element modelling of 3D orthogonal cutting experimental tests with the Coupled Eulerian-Langrangian (CEL) formulation. *Finite Elements in Analysis and Design*, *134*, 27–40.
16. Kalu-Uka, A., Ozoegwu, C., & Eberhard, P. (2023). 3D finite element simulation of Titanium alloy (Ti6Al4V) machining with harmonic endmill tools. *Proceedings in Applied Mathematics and Mechanics*, *22*(1), 1–6.
17. Malekian, M., Mostofa, M., & Park, S. (2012). Modelling of minimum uncut chip thickness in micro machining of aluminium. *Journal of Material Processing Technology*, *21*(3), 553–559.
18. Bergmann, B., Denkena, B., & Ko, J. (2015). Development of cutting edge geometries for hard milling operations. *CIRP Journal of Manufacturing Science Technology*, *8*, 43–52.
19. Thepsonthi, T. (2015). 3D finite element process simulation of micro-end milling Ti6Al4V titanium alloy: experimental validations on chip flow and tool wear. *Journal of Materials Processing Technology*, *221*, 128–145.
20. Lu, J., Chen, J., Fang, Q., Liu, B., Liu, Y., & Jin, T. (2016). Finite element simulation for Ti6Al4V alloy deformation near the exit of orthogonal cutting. *International Journal of Advanced Manufacturing Technology*, *85*, 2377–2388.
21. Rech, J., Arrazola, P., & Claudin, C. (2013). Characterisation of friction and heat partition coefficients at the tool-work material interface in cutting. *CIRP Annals-Manufacturing Technology*, *62*(1), 79–82.
22. Wu, H., Yan, X., & Luo, M. (2013). Cutting force prediction for circular end milling process. *Chinese Journal of Aeronautics*, *26*(4), 1057–1063.
23. Puls, H., Klocke, F., & Lung, D. (2014). Experimental investigation on friction under metal cutting conditions. *Wear*, *310*(1), 63–71.
24. Melkote, S., Grzesik, W., & Outeiro, J. (2017). Advances in material and friction data for modelling of metal machining. *CIRP Annals-Manufacturing Technology*, *66*(2), 731–754.
25. Davoudinejad, A., Chiappini, E., & Tirelli, S. (2015). Finite element simulation and validation of chip formation and cutting forces in dry and cryogenic cutting of Ti6Al4V. *Procedia Manufacturing*, *1*, 728–739.
26. He, Z., Zhang, X., & Ding, H. (2016). Comparison of residual stresses in cryogenic and dry machining of Inconel 718. *Procedia CIRP*, *46*, 19–22.
27. Rababah, M., Almagableh, A., & Aljarrah, M. (2013). Five-axis rake face grinding of end-mills with circular-arc generators. *Interactive Journal on Interactive Design and Manufacturing*, *11*, 93–101.

28. Waniker, N., & Dasarathi, G. (2015). Endmill helix angle selection. *Cadem Technologies PVT Ltd*, CNCTimes.com, November 17, 2015.
29. Moerman, K. (2018). GIBBON: The geometry and image-based bionengineering add-on. *Journal of Open Source Software*, *3*(22), 506.
30. Zhang, Y., Mabrouki, T., & Nelias, D. (2011). Chip formation in orthogonal cutting considering interface limiting stress and damage evolution based on fracture energy approach. *Finite Elements in Analysis and Design*, *47*(7), 850–863.
31. Denkena, B., Maa, P., & Schmidt, A. (2018). Thermomechanical deformation of complex workpieces in milling and drilling processes. *Thermal Effects in Complex Machining Processes*, Biermann, D., & Hollmann, F. (eds), Springer, pp. 219-250.
32. Papazafeiropoulos, G., Muniz-Calvente, M., & Martinez-Paneda, E. (2017). Abaqus2matlab: A suitable tool for finite element post-processing. *Advances in Engineering Software*, *105*, 9–16.
33. Upadhyay, V., Sonigra, S., & Daxini, S. (2021). Numerical analysis perspective in structural shape optimization: A review post 2000. *Advances in Engineering Software*, *155*(102992), 1–25.
34. Bendsoe, M., & Sigmund, O. (2002). Topology optimization. *Theory, methods and applications* (2nd ed.), Springer.
35. Sedlaczek, K., & Eberhard, P. (2006). Using augmented Lagrangian particle swarm optimization for constrained problems in engineering. *Structural and Multidisciplinary Optimization*, *32*, 277–286.
36. Simulia. (2020). ABAQUS/CAE user's manual. *Providence* version 7.6.
37. Wu, H., & Zhang, S. (2014). 3D FEM simulation of milling process for titanium alloy Ti6Al4V. *International Journal of Advanced Manufacturing Technology*, *71*, 1319–1326.
38. C., Maranhao, & J., (2010). Finite element modelling of machining of AISI 316 steel: Numerical simulation and experimental validation. *Simulation Modelling Practice and Theory*, *18*, 139–156.
39. Opoz, T., & Chen, X. (2022). Chip formation mechanism using finite element simulation. *Journal of Mechanical Engineering*, *62*(11), 636–646.
40. Xie, J., Bayoumi, A., & Zbib, H. (1996). A study on shear banding in chip formation of orthogonal machining. *International Journal of Machine Tools*, *36*(7), 835–847.
41. Mabrouki, T., Courbon, C., Zhang, Y., Rech, J., Nelias, D., Asad, M., Hamdi, H., Behaldi, S., & Salvatore, F. (2016). Some insights on the modelling of chip formation and its morphology during metal cutting operations. *Comptes Rendus Mecanique*, *344*(4-5), 335–354.
42. Batra, R., & Liu, D. (1990). Adiabatic shear banding in dynamic plane strain compression of a viscoplastic material. *International Journal of Plasticity*, *6*(2), 231–246.

How to cite this article: Kalu-Uka, A., Moerman, K., & Eberhard, P. (2024). Shape design optimization of a flat endmill tool. *Proceedings in Applied Mathematics and Mechanics*, *24*, e202400107.
https://doi.org/10.1002/pamm.202400107